Letter

Dzyaloshinskii-Moriya interaction torques and domain wall dynamics in van der Waals heterostructures

Jun Chen,* Churen Gui,* and Shuai Dong†
Key Laboratory of Quantum Materials and Devices of Ministry of Education, School of Physics, Southeast University, Nanjing 211189, China

(Received 23 May 2024; accepted 29 July 2024; published 7 August 2024)

Since the discovery of two-dimensional ferroelectric and ferromagnetic materials, the van der Waals (vdW) heterostructures constructed by ferroelectric and ferromagnetic monolayers soon became the ideal platforms to achieve converse magnetoelectric functions at the nanoscale, namely to use the electric field to control magnetization. In this Letter, by employing density functional theory calculations and dynamic simulations of the atomic spin model, we study the key role of the interfacial Dzyaloshinshii-Moriya interaction (DMI) in CrI_3-In_2Se_3 vdW heterostructures. Our work demonstrates feasible DMI torques pumped by ferroelectric switching, which can drive current-free and low-energy-consumption domain wall motion. Moreover, such an interfacial DMI can also significantly enlarge the Walker field in the magnetic-field-driven domain wall technique.

DOI: 10.1103/PhysRevB.110.L060406

Originating from spin-orbit coupling (SOC), the Dzyaloshinshii-Moriya interaction (DMI) plays a vital role in modern spintronics. By coupling neighbor spins in the antisymmetric form $H_D = \mathbf{D} \cdot (\mathbf{S}_i \times \mathbf{S}_j)$ [1], DMI can lead to many noncollinear spin textures, e.g., canting antiferromagnetism, chiral domain walls, as well as skyrmions [2–6]. It is well known that noncollinear spin textures usually produce nontrivial spin-electron scattering for transportation, which can contribute to topological (quantum) Hall effects and the motion of quasiparticles [7–12], facilitating functional manipulations at the nanoscale. Because the presence of DMI relies on the lack of space-inversion symmetry, DMI widely exists in those noncentrosymmetric magnetic materials. In particular, helimagnets such as $Mn_xFe_{1-x}Si$, $Fe_xCo_{1-x}Si$, and FeGe, in which the DMI causes spiral orders and/or skyrmions, have attracted much attention [13–17]. In addition, the asymmetric interfaces in artificial heterostructures or superlattices can also produce the interfacial DMI which leads to various emergent phenomena [3,18–23].

The reversibility of the DMI vector provides a promising route to control the chirality of magnetism. Multiferroics allows the coexistence of more than one ferroic order within a single phase material, which provides a platform to control the DMI vector via electric field or mechanical methods [24–26]. For some specific multiferroic systems, e.g., $BiFeO_3$, due to the locking between oxygen octahedral distortions and dipole moments, the DMI vector can be reversed by ferroelectric switching, leading to the flipping of the canting moment [27,28]. By reversing the DMI vector, topological spin textures or solitons can be manipulated [29–32]. Following this mechanism, Yu *et al.* demonstrated chirality-dependent skyrmion-skyrmion interactions [33].

The magnetic chirality also widely exists in domain walls, and thus DMI also plays an essential role in domain wall dynamics [34–39]. For example, reversal of the DMI vector can produce a dissipative transverse motion during the chirality switching, as demonstrated in perovskite multiferroics [40,41]. Comparing with the scenario based on current-dependent torques [42–44], such pure electric field control has the advantage of lower-energy consumption, which has been coined as a new class of "DMI torques" [45].

The van der Waals (vdW) heterostructures are ideal platforms to design electronic devices with controllable DMI, benefiting from their high-usage interfaces and easy control of stacking modes. As a widely studied system, the α-In_2Se_3 monolayer was theoretically predicted to be ferroelectric [46], which was then fabricated and confirmed in experiments [47]. After that, In_2Se_3-based heterostructures have been theoretically studied and designed for the nonvolatile electric field manipulation of various physical properties, including magnetism [48,49], topological states or spin textures [50–53], and band alignments and charge transfer [54,55]. Although domain walls have been attracting more and more attention in two-dimensional systems [56–58], the DMI control of domain wall dynamics remains less studied.

In this Letter, the DMI torques and domain wall dynamics of CrI_3-In_2Se_3 vdW heterostructures are studied. Our first-principles calculations indicate the interfacial DMI in the CrI_3 monolayer can be induced in these heterostructures and the full reversal of the DMI vector can be achieved in the $In_2Se_3/CrI_3/In_2Se_3$ sandwichlike heterostructure, which can generate DMI torques to drive the motion of domain walls. Furthermore, the existence of interfacial DMI can enlarge the critical field of the Walker breakdown in magnetic field-driven domain wall motion. Such magnetoelectric vdW

*These authors contributed equally to this work.
†Contact author: sdong@seu.edu.cn

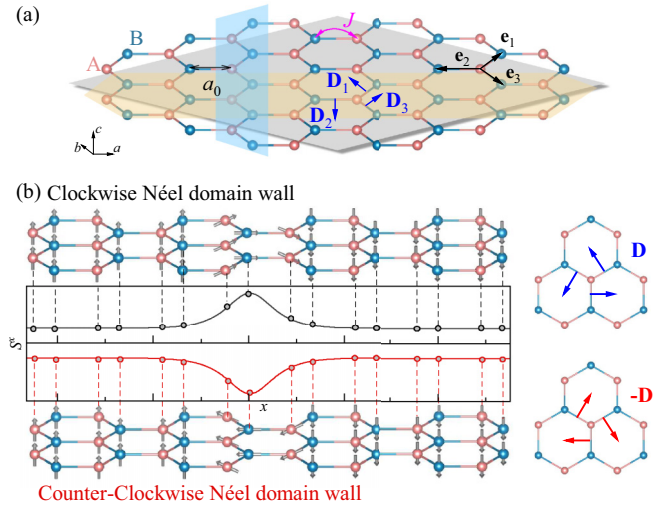

FIG. 1. (a) Schematic honeycomb lattice of magnetic layer stacking on a substrate, where the exchange interaction J and interfacial DMI vectors $\mathbf{D}_\mu$ ($\mu = 1, 2, 3$) are located at each nearest-neighboring bond between the A site and B site. $\mathbf{e}_\mu$: normalized axes. (b) Néel-type domain walls with clockwise or counterclockwise chiralities, plotted as one-dimensional coordinate functions of spin component $S^x(x)$. Such chirality can be determined by the DMI vectors correspondingly.

heterostructures shed light on low-energy-consuming domain wall nanoelectronic applications.

The CrI_3 monolayer is a well-recognized two-dimensional ferromagnetic sheet with a magnetic easy axis perpendicular to its plane [59]. The effective spin Hamiltonian for CrI_3's honeycomb lattice can be written as

$$H = -J\sum_{\langle i,j\rangle}\mathbf{S}_i\cdot\mathbf{S}_j - \sum_{\langle i,j\rangle}\mathbf{D}_{ij}\cdot(\mathbf{S}_i\times\mathbf{S}_j) - A\sum_i\left(S_i^z\right)^2, \quad (1)$$

where $\mathbf{S}$ is the normalized spin vector, i/j are site indices, and $\langle\,\rangle$ denotes nearest neighbors. As depicted in Fig. 1(a), the first term is the ferromagnetic exchange ($J > 0$), and the second term describes the interfacial DMI with the coefficient vector $\mathbf{D}$. Due to the inversion symmetry, $\mathbf{D} = \mathbf{0}$ for an isolated CrI_3 monolayer. However, the symmetry can be broken from the original D_{3d} to C_{3v} for the CrI_3 monolayer on a substrate, producing nonzero DMI vectors satisfy $\mathbf{D}_\mu = D\mathbf{e}_z\times\mathbf{e}_\mu$ ($\mu = 1, 2, 3$) as depicted in Fig. 1(a), where D is the amplitude of the DMI vector. The last term is the magnetocrystalline anisotropy with the easy axis along the z axis ($A > 0$).

Due to the presence of DMI, the magnetic domain walls should belong to the Néel-type with specific chirality [i.e., clockwise (CW) or counterclockwise (CCW)] to reduce the energy cost from DMI, as sketched in Fig. 1(b). In such a honeycomb lattice, although domain walls are possibly propagating along the zigzag or armchair directions, i.e., the shadow stripes in Fig. 1(a), they can be proved to be equivalent in the magnetic dynamics [60]. Then in the continuous limit, the model Hamiltonian for Néel-type domain walls propagating along the x axis can be expressed as

$$H = \int\left[\frac{J}{2}(\nabla\mathbf{S})^2 - D\mathbf{e}_y\cdot(\mathbf{S}\times\nabla\mathbf{S}) - \frac{4A}{3}(S^z)^2\right]dx. \quad (2)$$

Therefore, the domain wall can be described as $S^x = \mathrm{sech}(x/\Delta)$ with the characteristic width $\Delta = \sqrt{3J/8A}$ [61]. It is worthy to note that the effective width of the domain walls in the honeycomb lattice should be $\pi\Delta a_0$ [a_0 is the Cr-Cr distance as defined in Fig. 1(a)].

To obtain effective coefficients from real heterostructures, first-principles calculations based on density functional theory (DFT) are performed, and technical details of the calculations can be found in the Supplemental Material (SM) [60]. Both CrI_3 and In_2Se_3 monolayers are hexagonal lattices, as shown in Figs. 2(a) and 2(b), and their lattice constants are well matched by following the $(1\times1)/(\sqrt{3}\times\sqrt{3})$ stacking mode with a less than 0.5% mismatch. The CrI_3/In_2Se_3 bilayer and $In_2Se_3/CrI_3/In_2Se_3$ trilayer are considered. Here, the energetically most favorable stacking modes are displayed in Figs. 2(c)–2(f), while other stacking modes are discussed in SM [60]. The CrI_3/In_2Se_3 bilayer is polar despite the polarization direction of In_2Se_3. The $In_2Se_3/CrI_3/In_2Se_3$ trilayer can be polar or nonpolar, depending on the combination of polarizations of two In_2Se_3 layers, as shown in Figs. 2(e) and 2(f). For bilayer heterostructures $CrI_3/\uparrow$ and $CrI_3/\downarrow$ (here, $\uparrow$ or $\downarrow$ denotes the polarization direction in the In_2Se_3 layer), the energy is calculated as the function of the interlayer distance L. As shown in Fig. 2(g), their optimal distances $L_\uparrow$ and $L_\downarrow$ are only slightly different. A similar conclusion is also applicable to the trilayer heterostructures, in which the optimal L's slightly depend on the polarization of In_2Se_3 layers.

As aforementioned, the DMI can be induced by the proximity effects at the interfaces. Microscopically, DMI can originate from multiple factors, including the lattice distortion, orbital hybridization, electrostatic field, and charge transfer. Here, although the lattice distortions between Cr-I-Cr bonds are rather tiny after optimization, the charge density is significantly different between the upper I and lower I surfaces, due to the electrostatic field from In_2Se_3, as shown in Fig. 3(a). To calculate the DMI vector, two noncollinear magnetic orders with an identical exchange energy but opposite chiralities as depicted in Fig. 3(b), are calculated with SOC. The energy difference between these two states is only contributed by the DMI according to $D = (E_{CCW} - E_{CW})/4$.

All calculated coefficients including J, D, and A are summarized in Figs. 3(c) and 3(d). On one hand, comparing with monolayer CrI_3, the ferromagnetic exchange J is strengthened by 15%–28% in these heterostructures, while the magnetocrystalline anisotropy A is reduced by 0%–26%. Thus the ferromagnetism of CrI_3 should remain robust. On the other hand, nonzero $\mathbf{D}$'s appear only in those polar heterostructures. For bilayers, the amplitude of DMIs are estimated as 0.16 and 0.3 meV for $CrI_3/\uparrow$ and $CrI_3/\downarrow$, respectively. Interestingly, the sign of DMI does not change upon ferroelectric switching, implying that the single interface itself contributes to 0.23 meV while the reversible DMI contributes to 0.07 meV. For trilayers, the DMI is completely reversed from 0.08 meV in $\uparrow/CrI_3/\uparrow$ to -0.08 meV in $\downarrow/CrI_3/\downarrow$, while it is zero in $\uparrow/CrI_3/\downarrow$ or $\downarrow/CrI_3/\uparrow$ as expected from the inversion symmetry.

To study the spin dynamics of domain walls in the CrI_3 layer, we employed atomic simulations by solving

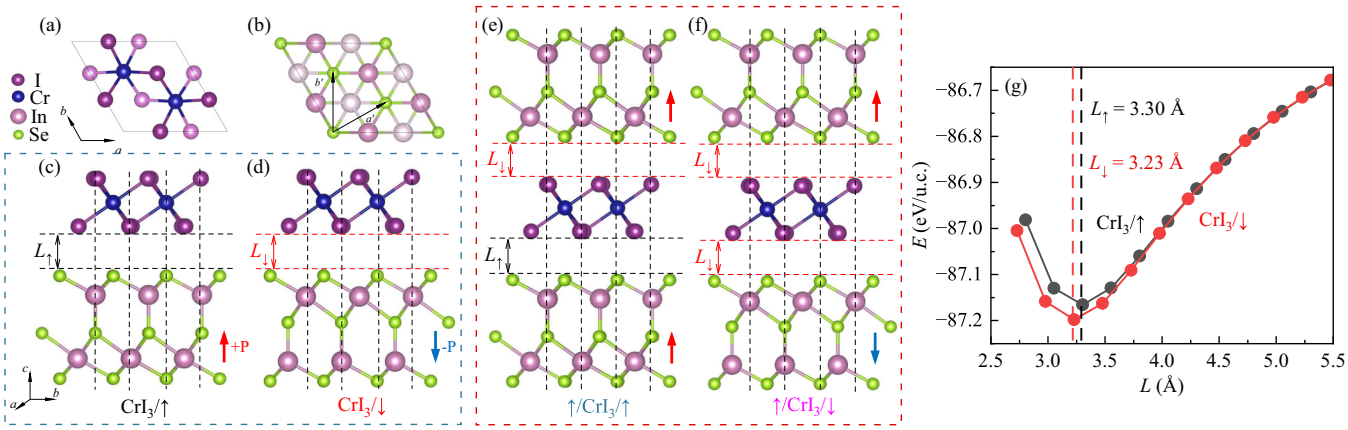

FIG. 2. Structures of CrI_3-In_2Se_3 heterostructures. (a), (b) Top view of CrI_3 monolayer (unit cell) and the $\sqrt{3} \times \sqrt{3}$ supercell of α-In_2Se_3. (c)–(f) Side views of heterostructures. (c) $CrI_3/\uparrow$, (d) $CrI_3/\downarrow$, (e) $\uparrow/CrI_3/\uparrow$, and (f) $\uparrow/CrI_3/\downarrow$, in which $\uparrow$ or $\downarrow$ denotes the polarization direction in the In_2Se_3 layer. (g) The total energy as a function of interlayer distance L for $CrI_3/\uparrow$ and $CrI_3/\downarrow$, where $L_\uparrow$ and $L_\downarrow$ represent their optimal interlayer distances.

Landau-Lifshitz-Gilbert (LLG) equation [61],

$$\frac{\partial \mathbf{S}}{\partial t} = \frac{\gamma}{\mu_s}\left(\mathbf{S} \times \frac{\partial H}{\partial \mathbf{S}}\right) + \alpha\left(\mathbf{S} \times \frac{\partial \mathbf{S}}{\partial t}\right), \tag{3}$$

where $\gamma = g\mu_B/\hbar$ is the gyromagnetic ratio. $\mu_s = 3\mu_B$ is the atomic magnetic moment for Cr^{3+}. The last term is for Gilbert damping with coefficient α, which is typically determined by electron spin resonance in experiments. A stripy honeycomb lattice $N = 600 \times 4$ is adopted, with periodic boundary conditions along the y direction and open boundary conditions along the x direction. The two x ends are fixed as spin up and spin down. The fourth-order Runge-Kutta method is used to solve the LLG equation to obtain the time-dependent evolution of spins.

In the trilayer heterostructures, the DMI vector can be reversed by flipping the polarization, i.e., from +0.08 to −0.08 meV, which is anticipated to pump the DMI torques for spin dynamics [40,45]. Here, we study an isolated domain wall at the honeycomb lattice, starting from a sharp boundary between the spin-up domain and spin-down domain. As shown in Fig. 4(a), due to the DMI ($D = 0.08$ meV) in $\uparrow/CrI_3/\uparrow$, the final stable state is a CW Néel-type domain wall. After the polarization flipping to $\downarrow/CrI_3/\downarrow$, the DMI energy will produce an effective field acting on the domain

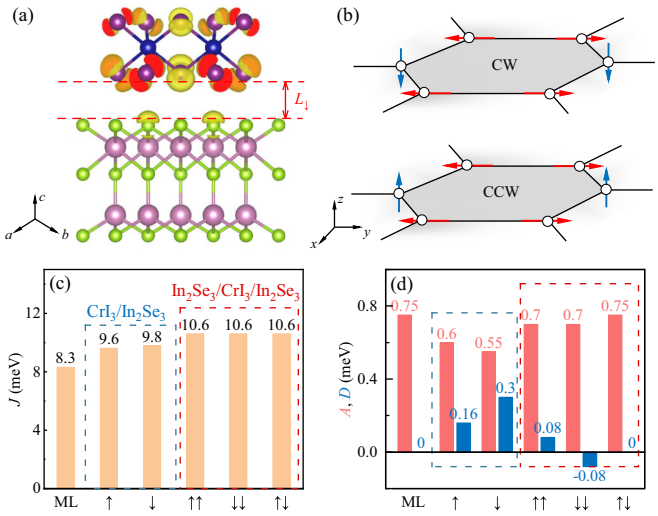

FIG. 3. (a) Charge redistribution between the upper I and lower I surfaces in $CrI_3/\downarrow$. The charge density is plotted near the Fermi level with range of $[-0.3, 0]$ eV with an isosurface level as 0.005 e/Å^3. (b) Noncollinear Cr-spin orders in a honeycomb lattice of the CrI_3 layer, where out-of-plane (blue arrows) and in-plane (red arrows) spins are in arrangements with different chiralities of CW or CCW. (c), (d) The exchange coefficient J, magnetocrystalline anisotropy A, and strength of the DMI vector $\mathbf{D}$ in the CrI_3 monolayer (ML) and CrI_3-In_2Se_3 heterostructures, where $\uparrow$ or $\downarrow$ denotes the polarization of the In_2Se_3 layer.

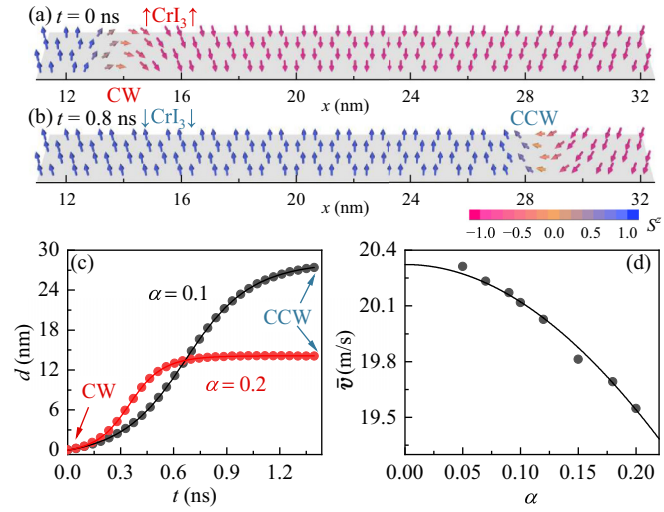

FIG. 4. DMI torque-driven domain wall motion. (a), (b) Snapshots of $\mathbf{S}$ texture with an isolated domain wall, before and after polarization flipping. The chirality of the domain wall is reversed from CW (at 0 ns) to CCW (at 0.8 ns). (c) The time-dependent domain wall position d with different damping coefficients. (d) The average velocities (solid circles) for the DMI torque-driven domain wall motion as a function of α, which can be well fitted using the formula $v_m(\alpha^2 + 1)^{-1}$.

wall, and thus pump a DMI torque as

$$\mathbf{\Gamma}_D = -\frac{2D\gamma}{\mu_s}(\mathbf{S}\cdot\mathbf{e}_y)\nabla\mathbf{S}, \tag{4}$$

which will reverse the chirality of the domain wall and induce a transverse motion as well. As shown in Fig. 4(b), with a large damping coefficient $\alpha = 0.2$, the domain wall moves by ∼15 nm along the x direction within 0.8 ns, accompanying its chirality reversal to CCW. This dynamic process with a smaller damping coefficient $\alpha = 0.1$ is also calculated for comparison. As shown in Fig. 4(c), the transverse motion distance d reaches ∼30 nm within ∼1.5 ns. The motion of the domain wall converges to stop gradually, thus it is not precise to define the motion time and the final distance d_s. In fact, for the honeycomb lattice, the DMI torque-driven domain wall motion can be well described by

$$d = \frac{a_0\Delta}{\alpha}\arctan\left[\sinh\left(\frac{t}{Q}\right)\right], \tag{5}$$

where $Q = 8\Delta(\alpha+\alpha^{-1})\mu_s/(3\pi\gamma D)$ denotes the characteristic time and the maximal moving distance is $d_s = a_0\Delta\pi/\alpha$. More details about the derivatives can be found in the Supplemental Material, and this kind of domain wall motion is similar to the "rolling-downhill"-type motion discovered in multiferroic perovskites [40]. All the simulation results are in perfect agreement with the theory, in which the moving distance is proportional to α^{-1} and independent on the strength of DMI. Here, we can define the effective time for the motion as $\sim 2\pi Q$, thus the average velocity can be calculated by $\bar{v} = 3a_0\pi\gamma D/[16(\alpha^2+1)\mu_s]$. The average velocity $\bar{v}$ increases with decreasing α and its maximal limitation is $v_m = 3a_0\pi\gamma D/16\mu_s$ when $\alpha \to 0$, in consistent with the simulation results as shown in Fig. 4(d). For the $In_2Se_3/CrI_3/In_2Se_3$ heterostructure, the maximal average velocity is estimated as ∼20 m/s, which is close to the typical velocity of magnetic field-driven ferromagnetic domain walls below 50 mT [35,62–64].

For completeness of domain wall motion, we also investigate the magnetic field-driven domain wall motion with different polarizations. Considering a magnetic field h along the z direction, the Zeeman energy term can be expressed as $H = -h\mu_s\sum_i \mathbf{e}_z\cdot\mathbf{S}_i$, which gives rise to a magnetic field torque as

$$\mathbf{\Gamma}_h = \gamma h\mathbf{e}_z\times\mathbf{S}. \tag{6}$$

The snapshots of domain wall dynamics in $CrI_3/\downarrow$ are displayed in Figs. 5(a) and 5(b), where the magnetic field torque together with Gilbert damping produce a dissipative torque to shift the domain wall and reduce the Zeeman energy. In this process, there is a critical field, called the Walker field h_W [62]. Below h_W, the dynamic process is mainly the steady motion, while it becomes a processional motion above h_W [Fig. 5(d)]. Here, the time-dependent domain wall motions under various magnetic fields are plotted in Figs. 5(c) and 5(d), which indicates $h_W \sim 152$ mT.

It is known that this h_W originates from the in-plane magnetic anisotropy. However, for the CrI_3 monolayer itself, the fully occupied t_{2g} orbitals at the Cr ion together with the

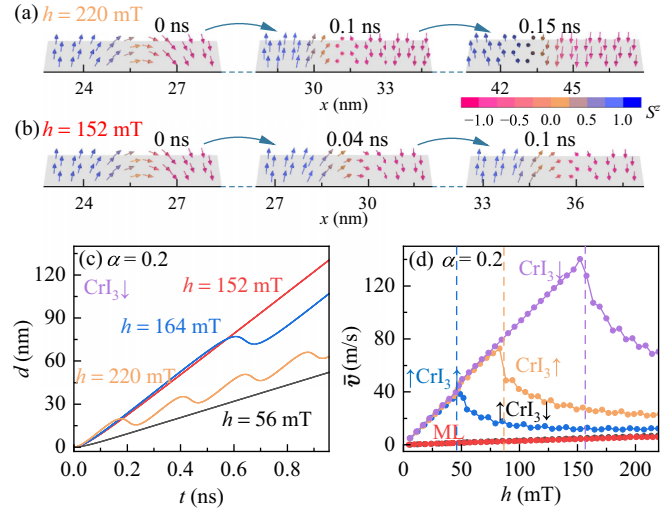

FIG. 5. Magnetic field-driven domain wall motion with $\alpha = 0.2$. (a), (b) Snapshots of the **S** textures in $CrI_3/\downarrow$ under different magnetic fields. Under a small field of 152 mT, the dynamic process is mainly the steady motion, while it becomes a processional motion under 220 mT. (c) Time-dependent domain wall positions under various magnetic fields. (d) Average velocity of domain wall motion as a function of magnetic field for monolayer CrI_3 and CrI_3-In_2Se_3 heterostructures, where dashed lines indicate the Walker fields calculated by Eq. (7).

D_{3d} point symmetry of the honeycomb lattice, preserve the in-plane symmetry and thus the in-plane magnetic anisotropy is almost zero [65–67], as confirmed in our calculations. Therefore, the magnetic in-plane anisotropy comes from the interfacial DMI. With the coarse-graining approximation, the Walker field can be derived as

$$h_W = \frac{3\pi\alpha D}{8\Delta\mu_s}, \tag{7}$$

which agrees very well with the above numerical value as shown in Fig. 5(d).

Without this interfacial DMI, e.g., in the CrI_3 monolayer, the domain wall motion can only be the processional motion, which leads to a velocity $v_p = a_0\alpha\gamma\Delta h/(1+\alpha^2)$. In heterostructures, below h_W, the domain wall motion reaches a final steady velocity v_s after a very short speeding duration (∼0.04 ns). This $v_s = a_0\gamma\Delta h/\alpha$ is much higher than the v_p. The numerical results of average velocity $\bar{v}$ are plotted in Fig. 5(d) as a function of magnetic field for different heterostructures. Compared with those $D = 0$ cases (CrI_3 monolayer and nonpolar $\uparrow/CrI_3/\downarrow$), all polar heterostructures have larger h_W and higher $\bar{v}$, as expected. In particular, below h_W, the velocity of domain wall can be up to ∼140 m/s for $CrI_3/\downarrow$, which is considerably large and similar to the gate-voltage effect in those magnetic film experiments [64,68].

In conclusion, by employing first-principles calculations and atomic spin dynamics simulations, we have studied the mechanism of interfacial DMI and domain wall dynamics in CrI_3-In_2Se_3 heterostructures. We have demonstrated the DMI torques can be pumped into $In_2Se_3/CrI_3/In_2Se_3$ trilayer

heterostructures by polarization flipping, which contributes an efficient domain wall motion without either magnetic field or current. Furthermore, the existing and tunable DMI within heterostructures also plays an important role in improving the critical Walker field for magnetic field-driven domain wall motion, exhibiting a tunable and nonvolatile bias effect. In addition, our results are completely portable to other vdW heterostructures, which can be described by the effective spin model as well. Our results have performed rich manipulations of magnetic domain walls, which can be achieved in magnetoelectric vdW heterostructures.

This work was supported by the National Natural Science Foundation of China (Grants No. 12325401 and No. 12274069), China Scholarship Council, Postgraduate Research & Practice Innovation Program of Jiangsu Province (Grant No. KYCX21_0079), and the Big Data Computing Center of Southeast University.

[1] T. Moriya, Anisotropic superexchange interaction and weak ferromagnetism, Phys. Rev. **120**, 91 (1960).
[2] P. Bak and M. H. Jensen, Theory of helical magnetic structures and phase transitions in MnSi and FeGe, J. Phys. C: Solid State Phys. **13**, L881 (1980).
[3] M. Heide, G. Bihlmayer, and S. Blügel, Dzyaloshinskii-Moriya interaction accounting for the orientation of magnetic domains in ultrathin films: Fe/W(110), Phys. Rev. B **78**, 140403(R) (2008).
[4] C. Pappas, E. Lelièvre-Berna, P. Falus, P. M. Bentley, E. Moskvin, S. Grigoriev, P. Fouquet, and B. Farago, Chiral paramagnetic skyrmion-like phase in MnSi, Phys. Rev. Lett. **102**, 197202 (2009).
[5] S. Mühlbauer, B. Binz, F. Jonietz, C. Pfleiderer, A. Rosch, A. Neubauer, R. Georgii, and P. Böni, Skyrmion lattice in a chiral magnet, Science **323**, 915 (2009).
[6] S. D. Yi, S. Onoda, N. Nagaosa, and J. H. Han, Skyrmions and anomalous Hall effect in a Dzyaloshinskii-Moriya spiral magnet, Phys. Rev. B **80**, 054416 (2009).
[7] K. Ohgushi, S. Murakami, and N. Nagaosa, Spin anisotropy and quantum Hall effect in the kagomé lattice: Chiral spin state based on a ferromagnet, Phys. Rev. B **62**, R6065 (2000).
[8] Y. Taguchi, Y. Oohara, H. Yoshizawa, N. Nagaosa, and Y. Tokura, Spin chirality, Berry phase, and anomalous Hall effect in a frustrated ferromagnet, Science **291**, 2573 (2001).
[9] S. Onoda and N. Nagaosa, Spin chirality fluctuations and anomalous Hall effect in itinerant ferromagnets, Phys. Rev. Lett. **90**, 196602 (2003).
[10] S. S. Parkin, M. Hayashi, and L. Thomas, Magnetic domain-wall racetrack memory, Science **320**, 190 (2008).
[11] J. Iwasaki, M. Mochizuki, and N. Nagaosa, Universal current-velocity relation of skyrmion motion in chiral magnets, Nat. Commun. **4**, 1463 (2013).
[12] J. Barker and O. A. Tretiakov, Static and dynamical properties of antiferromagnetic skyrmions in the presence of applied current and temperature, Phys. Rev. Lett. **116**, 147203 (2016).
[13] C. Pfleiderer, T. Adams, A. Bauer, W. Biberacher, B. Binz, F. Birkelbach, P. Böni, C. Franz, R. Georgii, M. Janoschek, F. Jonietz, T. Keller, R. Ritz, S. Mühlbauer, W. Münzer, A. Neubauer, B. Pedersen, and A. Rosch, Skyrmion lattices in metallic and semiconducting B20 transition metal compounds, J. Phys.: Condens. Matter **22**, 164207 (2010).
[14] H. Wilhelm, M. Baenitz, M. Schmidt, U. K. Rößler, A. A. Leonov, and A. N. Bogdanov, Precursor phenomena at the magnetic ordering of the cubic helimagnet FeGe, Phys. Rev. Lett. **107**, 127203 (2011).
[15] X. Yu, N. Kanazawa, Y. Onose, K. Kimoto, W. Zhang, S. Ishiwata, Y. Matsui, and Y. Tokura, Near room-temperature formation of a skyrmion crystal in thin-films of the helimagnet FeGe, Nat. Mater. **10**, 106 (2011).
[16] R. Viennois, C. Reibel, D. Ravot, R. Debord, and S. Pailhès, Observation of various magnetic-field-induced states in B20 cubic MnGe, Europhys. Lett. **111**, 17008 (2015).
[17] D. McGrouther, R. J. Lamb, M. Krajnak, S. McFadzean, S. McVitie, R. L. Stamps, A. O. Leonov, A. N. Bogdanov, and Y. Togawa, Internal structure of hexagonal skyrmion lattices in cubic helimagnets, New J. Phys. **18**, 095004 (2016).
[18] M. Bode, M. Heide, K. Von Bergmann, P. Ferriani, S. Heinze, G. Bihlmayer, A. Kubetzka, O. Pietzsch, S. Blügel, and R. Wiesendanger, Chiral magnetic order at surfaces driven by inversion asymmetry, Nature (London) **447**, 190 (2007).
[19] O. Boulle, J. Vogel, H. Yang, S. Pizzini, D. De Souza Chaves, A. Locatelli, T. O. Menteş, A. Sala, L. D. Buda-Prejbeanu, O. Klein, M. Belmeguenai, Y. Roussigné, A. Stashkevich, S. M. Chérif, L. Aballe, M. Foerster, M. Chshiev, S. Auffret, I. M. Miron, and G. Gaudin, Room-temperature chiral magnetic skyrmions in ultrathin magnetic nanostructures, Nat. Nanotechnol. **11**, 449 (2016).
[20] S. Woo, K. Litzius, B. Krüger, M.-Y. Im, L. Caretta, K. Richter, M. Mann, A. Krone, R. M. Reeve, M. Weigand, P. Agrawal, I. Lemesh, M.-A. Mawass, P. Fischer, M. Kläui, and G. S. D. Beach, Observation of room-temperature magnetic skyrmions and their current-driven dynamics in ultrathin metallic ferromagnets, Nat. Mater. **15**, 501 (2016).
[21] A. Fert, N. Reyren, and V. Cros, Magnetic skyrmions: Advances in physics and potential applications, Nat. Rev. Mater. **2**, 17031 (2017).
[22] H. Yang, G. Chen, A. A. C. Cotta, A. T. N'Diaye, S. A. Nikolaev, E. A. Soares, W. A. A. Macedo, K. Liu, A. K. Schmid, A. Fert, and M. Chshiev, Significant Dzyaloshinskii-Moriya interaction at graphene-ferromagnet interfaces due to the Rashba effect, Nat. Mater. **17**, 605 (2018).
[23] A. Soumyanarayanan, N. Reyren, A. Fert, and C. Panagopoulos, Emergent phenomena induced by spin-orbit coupling at surfaces and interfaces, Nature (London) **539**, 509 (2016).
[24] S. Dong, J.-M. Liu, S.-W. Cheong, and Z. F. Ren, Multiferroic materials and magnetoelectric physics: Symmetry, entanglement, excitation, and topology, Adv. Phys. **64**, 519 (2015).
[25] S.-W. Cheong and M. Mostovoy, Multiferroics: A magnetic twist for ferroelectricity, Nat. Mater. **6**, 13 (2007).
[26] S. Dong, H. J. Xiang, and E. Dagotto, Magnetoelectricity in multiferroics: A theoretical perspective, Natl. Sci. Rev. **6**, 629 (2019).
[27] J. T. Heron, M. Trassin, K. Ashraf, M. Gajek, Q. He, S. Y. Yang, D. E. Nikonov, Y.-H. Chu, S. Salahuddin, and R. Ramesh, Electric-field-induced magnetization reversal in a

ferromagnet-multiferroic heterostructure, Phys. Rev. Lett. **107**, 217202 (2011).

[28] J. T. Heron, J. L. Bosse, Q. He, Y. Gao, M. Trassin, L. Ye, J. D. Clarkson, C. Wang, J. Liu, S. Salahuddin, D. C. Ralph, D. G. Schlom, J. Íñiguez, B. D. Huey, and R. Ramesh, Deterministic switching of ferromagnetism at room temperature using an electric field, Nature (London) **516**, 370 (2014).

[29] T. Srivastava, M. Schott, R. Juge, V. Křižáková, M. Belmeguenai, Y. Roussigné, A. Bernand-Mantel, L. Ranno, S. Pizzini, S.-M. Chérif, A. Stashkevich, S. Auffret, O. Boulle, G. Gaudin, M. Chshiev, C. Baraduc, and H. Béa, Large-voltage tuning of Dzyaloshinskii-Moriya interactions: A route toward dynamic control of skyrmion chirality, Nano Lett. **18**, 4871 (2018).

[30] J. Liang, Q. Cui, and H. Yang, Electrically switchable Rashba-type Dzyaloshinskii-Moriya interaction and skyrmion in two-dimensional magnetoelectric multiferroics, Phys. Rev. B **102**, 220409(R) (2020).

[31] C. Xu, P. Chen, H. Tan, Y. Yang, H. Xiang, and L. Bellaiche, Electric-field switching of magnetic topological charge in type-I multiferroics, Phys. Rev. Lett. **125**, 037203 (2020).

[32] B. Dai, D. Wu, S. A. Razavi, S. Xu, H. He, Q. Shu, M. Jackson, F. Mahfouzi, H. Huang, Q. Pan, Y. Cheng, T. Qu, T. Wang, L. Tai, K. Wong, N. Kioussis, and K. L. Wang, Electric-field control of skyrmions in multiferroic heterostructure via magnetoelectric coupling, Nat. Commun. **12**, 322 (2021).

[33] D. Yu, H. Yang, M. Chshiev, and A. Fert, Skyrmions-based logic gates in one single nanotrack completely reconstructed via chirality barrier, Natl. Sci. Rev. **9**, nwac021 (2022).

[34] A. Thiaville, S. Rohart, E. Jué, V. Cros, and A. Fert, Dynamics of Dzyaloshinskii domain walls in ultrathin magnetic films, Europhys. Lett. **100**, 57002 (2012).

[35] Y. Yoshimura, K.-J. Kim, T. Taniguchi, T. Tono, K. Ueda, R. Hiramatsu, T. Moriyama, K. Yamada, Y. Nakatani, and T. Ono, Soliton-like magnetic domain wall motion induced by the interfacial Dzyaloshinskii-Moriya interaction, Nat. Phys. **12**, 157 (2016).

[36] J. Vandermeulen, S. A. Nasseri, B. Van De Wiele, G. Durin, B. Van Waeyenberge, and L. Dupré, The effect of Dzyaloshinskii-Moriya interaction on field-driven domain wall dynamics analysed by a semi-analytical approach, J. Phys. D: Appl. Phys. **49**, 465003 (2016).

[37] J. P. Garcia, A. Fassatoui, M. Bonfim, J. Vogel, A. Thiaville, and S. Pizzini, Magnetic domain wall dynamics in the precessional regime: Influence of the Dzyaloshinskii-Moriya interaction, Phys. Rev. B **104**, 014405 (2021).

[38] J. Brandão, S. Azzawi, A. T. Hindmarch, and D. Atkinson, Understanding the role of damping and Dzyaloshinskii-Moriya interaction on dynamic domain wall behaviour in platinum-ferromagnet nanowires, Sci. Rep. **7**, 4569 (2017).

[39] Y. Ba, S. Zhuang, Y. Zhang, Y. Wang, Y. Gao, H. Zhou, M. Chen, W. Sun, Q. Liu, G. Chai, J. Ma, Y. Zhang, H. Tian, H. Du, W. Jiang, C. Nan, J.-M. Hu, and Y. Zhao, Electric field manipulation of spin chirality and skyrmion dynamic, Sci. Adv. **9**, eade2441 (2023).

[40] J. Chen and S. Dong, Manipulation of magnetic domain walls by ferroelectric switching: Dynamic magnetoelectricity at the nanoscale, Phys. Rev. Lett. **126**, 117603 (2021).

[41] S. Li, X. Lin, P. Li, S. Zhao, Z. Si, G. Wei, B. Koopmans, R. Lavrijsen, and W. Zhao, Ultralow power and shifting-discretized magnetic racetrack memory device driven by chirality switching and spin current, ACS Appl. Mater. Interfaces **15**, 39946 (2023).

[42] J. C. Slonczewski, Current-driven excitation of magnetic multilayers, J. Magn. Magn. Mater. **159**, L1 (1996).

[43] L. Berger, Emission of spin waves by a magnetic multilayer traversed by a current, Phys. Rev. B **54**, 9353 (1996).

[44] J. Železný, H. Gao, K. Výborný, J. Zemen, J. Mašek, A. Manchon, J. Wunderlich, J. Sinova, and T. Jungwirth, Relativistic Néel-order fields induced by electrical current in antiferromagnets, Phys. Rev. Lett. **113**, 157201 (2014).

[45] D. Yu, Y. Ga, J. Liang, C. Jia, and H. Yang, Voltage-controlled Dzyaloshinskii-Moriya interaction torque switching of perpendicular magnetization, Phys. Rev. Lett. **130**, 056701 (2023).

[46] W. Ding, J. Zhu, Z. Wang, Y. Gao, D. Xiao, Y. Gu, Z. Zhang, and W. Zhu, Prediction of intrinsic two-dimensional ferroelectrics in In_2Se_3 and other III_2-VI_3 van der Waals materials, Nat. Commun. **8**, 14956 (2017).

[47] Y. Zhou, D. Wu, Y. Zhu, Y. Cho, Q. He, X. Yang, K. Herrera, Z. Chu, Y. Han, M. C. Downer, H. Peng, and K. Lai, Out-of-plane piezoelectricity and ferroelectricity in layered α-In_2Se_3 nanoflakes, Nano Lett. **17**, 5508 (2017).

[48] H.-X. Cheng, J. Zhou, C. Wang, W. Ji, and Y.-N. Zhang, Nonvolatile electric field control of magnetism in bilayer CrI_3 on monolayer In_2Se_3, Phys. Rev. B **104**, 064443 (2021).

[49] Y. Wang, X. Xu, X. Zhao, W. Ji, Q. Cao, S. Li, and Y. Li, Switchable half-metallicity in A-type antiferromagnetic NiI_2 bilayer coupled with ferroelectric In_2Se_3, npj Comput. Mater. **8**, 218 (2022).

[50] J.-J. Zhang, D. Zhu, and B. I. Yakobson, Heterobilayer with ferroelectric switching of topological state, Nano Lett. **21**, 785 (2021).

[51] K. Huang, D.-F. Shao, and E. Y. Tsymbal, Ferroelectric control of magnetic skyrmions in two-dimensional van der Waals heterostructures, Nano Lett. **22**, 3349 (2022).

[52] Z. Shen, S. Dong, and X. Yao, Manipulation of magnetic topological textures via perpendicular strain and polarization in van der waals magnetoelectric heterostructures, Phys. Rev. B **108**, L140412 (2023).

[53] Z.-Q. Wang, F. Xue, L. Qiu, Z. Wang, R. Wu, and Y. Hou, Switching intrinsic magnetic skyrmions with controllable magnetic anisotropy in van der Waals multiferroic heterostructures, Nano Lett. **24**, 4117 (2024).

[54] C. Hu, J. Chen, E. Du, W. Ju, Y. An, and S.-J. Gong, Ferroelectric control of band alignments and magnetic properties in the two-dimensional multiferroic VSe_2/In_2Se_3, J. Phys.: Condens. Matter **34**, 425801 (2022).

[55] K. Zhang, X. Wang, and W. Mi, Ferroelectric control of half-metallicity in A-type antiferromagnetic GdI_2 bilayer coupled with ferroelectric In_2Se_3, Physica E Low Dimens. Syst. Nanostruct. **155**, 115836 (2024).

[56] D. A. Wahab, M. Augustin, S. M. Valero, W. Kuang, S. Jenkins, E. Coronado, I. V. Grigorieva, I. J. Vera-Marun, E. Navarro-Moratalla, R. F. L. Evans, K. S. Novoselov, and E. J. G. Santos, Quantum rescaling, domain metastability, and hybrid domain-walls in 2D CrI_3 magnets, Adv. Mater. **33**, 2004138 (2021).

[57] D. Abdul-Wahab, E. Iacocca, R. F. L. Evans, A. Bedoya-Pinto, S. Parkin, K. S. Novoselov, and E. J. G. Santos, Domain wall dynamics in two-dimensional van der Waals ferromagnets, Appl. Phys. Rev. **8**, 041411 (2021).

[58] I. M. Alliati, R. F. L. Evans, K. S. Novoselov, and E. J. G. Santos, Relativistic domain-wall dynamics in van der Waals antiferromagnet $MnPS_3$, npj Comput. Mater. **8**, 3 (2022).

[59] B. Huang, G. Clark, E. Navarro-Moratalla, D. R. Klein, R. Cheng, K. L. Seyler, D. Zhong, E. Schmidgall, M. A. McGuire, D. H. Cobden, W. Yao, D. Xiao, P. Jarillo-Herrero, and X. Xu, Layer-dependent ferromagnetism in a van der Waals crystal down to the monolayer limit, Nature (London) **546**, 270 (2017).

[60] See Supplemental Material at http://link.aps.org/supplemental/10.1103/PhysRevB.110.L060406 for more details about first-principles calculations including a discussion of stacking modes for CrI_3-In_2Se_3 heterostructures, the parameters of lattices, self-consistent calculations and extractions of magnetic coefficients, and the effective continuous model and derivatives of the coarse-graining approach for domain wall motions, which includes Refs. [34,48,61,62,69–75].

[61] L. D. Landau and E. Lifshitz, On the theory of the dispersion of magnetic permeability in ferromagnetic bodies, Phys. Z. Sowjet. **8**, 153 (1935).

[62] N. L. Schryer and L. R. Walker, The motion of 180° domain walls in uniform dc magnetic fields, J. Appl. Phys. **45**, 5406 (1974).

[63] E. Jué, A. Thiaville, S. Pizzini, J. Miltat, J. Sampaio, L. D. Buda-Prejbeanu, S. Rohart, J. Vogel, M. Bonfim, O. Boulle, S. Auffret, I. M. Miron, and G. Gaudin, Domain wall dynamics in ultrathin Pt/Co/AlOx microstrips under large combined magnetic fields, Phys. Rev. B **93**, 014403 (2016).

[64] W. Lin, N. Vernier, G. Agnus, K. Garcia, B. Ocker, W. Zhao, E. E. Fullerton, and D. Ravelosona, Universal domain wall dynamics under electric field in Ta/CoFeB/MgO devices with perpendicular anisotropy, Nat. Commun. **7**, 13532 (2016).

[65] S. Jiang, L. Li, Z. Wang, K. F. Mak, and J. Shan, Controlling magnetism in 2D CrI_3 by electrostatic doping, Nat. Nanotechnol. **13**, 549 (2018).

[66] L. Webster and J.-A. Yan, Strain-tunable magnetic anisotropy in monolayer $CrCl_3$, $CrBr_3$, and CrI_3, Phys. Rev. B **98**, 144411 (2018).

[67] J. Kim, K.-W. Kim, B. Kim, C.-J. Kang, D. Shin, S.-H. Lee, B.-C. Min, and N. Park, Exploitable magnetic anisotropy of the two-dimensional magnet CrI_3, Nano Lett. **20**, 929 (2020).

[68] A. Schellekens, A. Van Den Brink, J. Franken, H. Swagten, and B. Koopmans, Electric-field control of domain wall motion in perpendicularly magnetized materials, Nat. Commun. **3**, 847 (2012).

[69] G. Kresse and J. Furthmüller, Efficiency of *ab-initio* total energy calculations for metals and semiconductors using a plane-wave basis set, Comput. Mater. Sci. **6**, 15 (1996).

[70] G. Kresse and J. Furthmüller, Efficient iterative schemes for *ab initio* total-energy calculations using a plane-wave basis set, Phys. Rev. B **54**, 11169 (1996).

[71] J. Hafner, *Ab-initio* simulations of materials using VASP: Density-functional theory and beyond, J. Comput. Chem. **29**, 2044 (2008).

[72] J. L. Lado and J. Fernández-Rossier, On the origin of magnetic anisotropy in two dimensional CrI_3, 2D Mater. **4**, 035002 (2017).

[73] N. Sivadas, S. Okamoto, X. Xu, C. J. Fennie, and D. Xiao, Stacking-dependent magnetism in bilayer CrI_3, Nano Lett. **18**, 7658 (2018).

[74] J. P. Perdew, K. Burke, and M. Ernzerhof, Generalized gradient approximation made simple, Phys. Rev. Lett. **77**, 3865 (1996).

[75] S. L. Dudarev, G. A. Botton, S. Y. Savrasov, C. Humphreys, and A. P. Sutton, Electron-energy-loss spectra and the structural stability of nickel oxide: An LSDA+U study, Phys. Rev. B **57**, 1505 (1998).